THE UNIVERSITY of EDINBURGH

Edinburgh Research Explorer

Internally consistent thermodynamic database for iron to the Earth's core conditions

Citation for published version:
Komabayashi, T & Fei, Y 2010, 'Internally consistent thermodynamic database for iron to the Earth's core conditions', *Journal of Geophysical Research*, vol. 115, no. B3, B03202, pp. 1-12. https://doi.org/10.1029/2009JB006442

Digital Object Identifier (DOI):
10.1029/2009JB006442

Link:
Link to publication record in Edinburgh Research Explorer

Document Version:
Publisher's PDF, also known as Version of record

Published In:
Journal of Geophysical Research

Publisher Rights Statement:
Published in Journal of Geophysical Research: Solid Earth by American Geophysical Union (2010)

General rights
Copyright for the publications made accessible via the Edinburgh Research Explorer is retained by the author(s) and / or other copyright owners and it is a condition of accessing these publications that users recognise and abide by the legal requirements associated with these rights.

Take down policy
The University of Edinburgh has made every reasonable effort to ensure that Edinburgh Research Explorer content complies with UK legislation. If you believe that the public display of this file breaches copyright please contact openaccess@ed.ac.uk providing details, and we will remove access to the work immediately and investigate your claim.

Download date: 04. May. 2023

JOURNAL OF GEOPHYSICAL RESEARCH, VOL. 115, B03202, doi:10.1029/2009JB006442, 2010

Click Here for Full Article

Internally consistent thermodynamic database for iron to the Earth's core conditions

Tetsuya Komabayashi[1,2] and Yingwei Fei[1]

Received 8 March 2009; revised 1 September 2009; accepted 25 September 2009; published 13 March 2010.

[1] An internally consistent thermodynamic database for pure iron has been established to pressures (P) up to 360 GPa and temperatures (T) up to 7000 K from existing static experimental data and thermochemical measurements. The database includes body-centered cubic (BCC) phases (α or δ phase), the face-centered cubic (FCC) phase (γ phase), the hexagonal close-packed (HCP) phase (ε phase), and the liquid phase. We describe fundamental thermodynamic relations as the Gibbs free energy divided into thermochemical and thermophysical terms. The thermochemical data were evaluated from existing metallurgy databases together with experimentally determined phase relations. The thermophysical term is obtained from the pressure-volume-temperature equations of state (EoS) for the phases. We constructed an EoS of the FCC phase from our recent internally-heated diamond anvil cell (DAC) experimental data and assessed the EoS of the liquid phase from existing laser-heated DAC experiments together with density data at P = 1 bar, 0.2 GPa, and along the Hugoniot. The HCP-FCC-liquid triple point is located at P = 90 GPa and T = 2800 K. The calculated melting temperature of HCP iron at the inner core boundary (P = 330 GPa) is 4900 K and the density change at melting is −1.2%. The core density deficits at the inner core boundary are 8.1 wt.% and 5.3 wt.% for the liquid outer core and solid inner core, respectively. The calculated melting temperature is much lower than that from dynamic shock wave experiments, suggesting that the HCP structure may not be stable in the inner core. We included a hypothetical high-pressure BCC phase which could be stabilized above 220 GPa by a solid-solid transition of high-P BCC-HCP phases. This hypothetical BCC phase should have a large entropy to give a high melting temperature in order to reconcile the existing discrepancies between the static and shock wave experimental studies.

Citation: Komabayashi, T., and Y. Fei (2010), Internally consistent thermodynamic database for iron to the Earth's core conditions, *J. Geophys. Res.*, *115*, B03202, doi:10.1029/2009JB006442.

1. Introduction

[2] Iron is the primary component of the Earth's core. Its phase relations have been a focus of researches for the last 50 years [e.g., *Li and Fei*, 2007, and references therein]. However, consensus on the phase relations of iron is limited to a narrow low-P and low-T range which is far from the Earth's core conditions (P = 135–364 GPa, T = 4000–7000 K). Figure 1 is a summary of previous experimental and theoretical interpretations of the iron phase diagram. At approximately P = 10 GPa and T = 800 K, there is a triple point (TP-1) of α (magnetic body-centered cubic, BCC), γ (face-centered cubic, FCC), and ε (hexagonal close-packed, HCP) phases. From this TP-1 toward the high-P-T region, the FCC-HCP boundary divides the stability fields of FCC and HCP iron. The location of the FCC-HCP boundary has been controversial among static experimental studies using a laser-heated diamond anvil cell (DAC). The issues include (1) the P-T slope which determines the P-T location of a second triple point (TP-2) of FCC, HCP, and liquid phases [*Boehler*, 1993; *Shen et al.*, 1998; *Ma et al.*, 2004] and (2) the presence or absence of a β phase with either a double hexagonal close-packed (DHCP) or an orthorhombic structure as a high-temperature phase above T = 1200 K and P = 30 GPa [*Saxena et al.*, 1995; *Yoo et al.*, 1995; *Andrault et al.*, 1997; *Shen et al.*, 1998; *Kubo et al.*, 2003]. Very recently, we revisited this transition by using a newly developed internally resistive heated DAC together with an angle-dispersive high resolution X-ray diffraction method [*Komabayashi et al.*, 2009]. We did not observe any evidence for the β phase along the FCC-HCP boundary. The precisely determined P-T location of the TP-2 is at P = 88 GPa and T = 2800 K which is in general agreement with the result of *Boehler* [1993].

[3] There has also been a lack of consensus among the existing studies regarding the melting curve of iron at high pressure which provides a constraint on the temperature at the liquid outer core–solid inner core boundary

[1]Geophysical Laboratory, Carnegie Institution of Washington, Washington, D. C., USA.
[2]Department of Earth and Planetary Sciences, Tokyo Institute of Technology, Tokyo, Japan.

Copyright 2010 by the American Geophysical Union.
0148-0227/10/2009JB006442

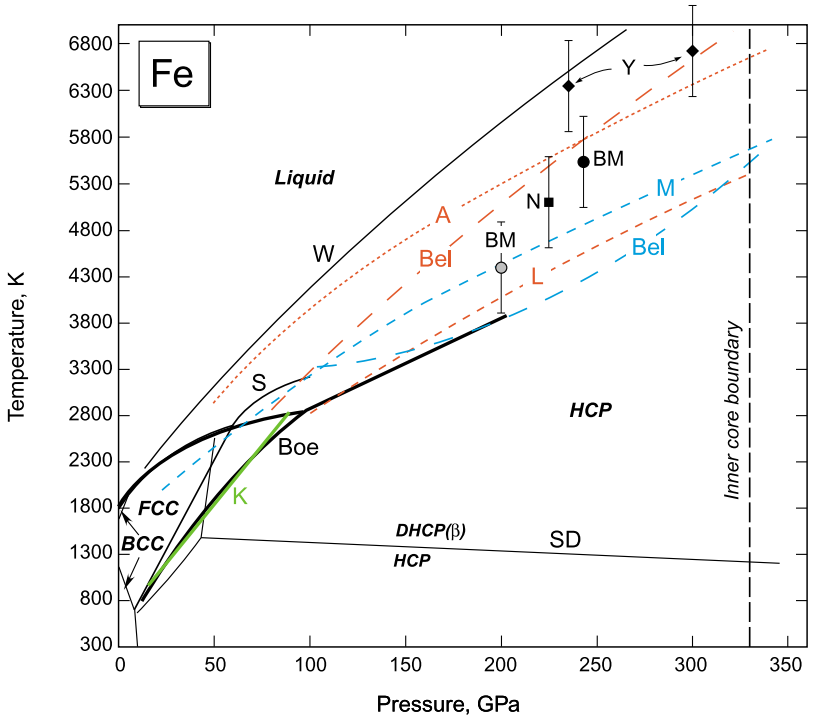

Figure 1. Summary of previous studies on the phase relations of pure iron. Solid lines and broken lines are experimentally and theoretically constrained boundaries, respectively. W, *Williams et al.* [1987]; S, *Shen et al.* [1998]; Boe, *Boehler et al.* [1990] and *Boehler* [1993]; SD, *Saxena and Dubrovinsky* [2000]; K, *Komabayashi et al.* [2009]; A, *Alfè et al.* [1999]; L, *Laio et al.* [2000]; M (FCC-HCP transition), *Mikhaylushkin et al.* [2007]; Bel (red) (HCP melting), *Belonoshko et al.* [2000]; Bel (blue) (high-*P* BCC-HCP transition), *Belonoshko et al.* [2003]. The black and grey solid symbols are melting point and solid-solid transition, respectively, observed in the shock wave experiments. BM, *Brown and McQueen* [1986]; Y, *Yoo et al.* [1993]; N, *Nguyen and Holmes* [2004]. BCC, body-centered cubic phase; FCC, face-centered cubic phase; HCP, hexagonal close-packed phase; DHCP, double HCP phase.

(ICB) at P = 330 GPa. *Boehler* [1993] reported a melting temperature of 3800 K at P = 200 GPa by static experiments. An extension of *Boehler*'s [1993] melting curve yielded 5100 K at the ICB. In contrast, shock wave experiments by *Brown and McQueen* [1986] showed much higher melting temperatures (5500 K at P = 243 GPa). Another shock wave study which measured temperature directly also indicated high melting temperatures (6350 K at 235 GPa and 6720 K at 300 GPa) [*Yoo et al.*, 1993]. *Yoo et al.*'s [1993] results would yield a melting temperature of 6830 K at the ICB. *Nguyen and Holmes* [2004] reported somewhat lower melting temperature than those previous shock wave studies. A theoretical study of the melting curves of iron phases based on the embedded atom method [*Belonoshko and Ahuja*, 1997] resulted in a melting curve for the HCP phase in reasonable agreement with the shock wave data. From first-principles calculations, *Alfè et al.* [1999] and *Belonoshko et al.* [2000] showed that the calculated melting curve is more consistent with the shock wave data [*Brown and McQueen*, 1986; *Yoo et al.*, 1993] whereas *Laio et al.* [2000] reported a melting curve that is consistent with the static DAC data [*Boehler*, 1993] (Figure 1). On the other hand, O. L. Anderson and his coworkers took a thermodynamic approach to this problem (see *Anderson* [1995] for review). *Anderson and Isaak* [2000] calculated the melting curve of the HCP phase, on the basis of the Gilvarry rule [*Gilvarry*, 1956]. They synthesized a plausible physical model from available physical parameters for iron melting. The calculated melting temperature at P = 330 GPa was about 5800 K and they concluded that the melting behavior of the HCP iron is consistent with the shock wave data [*Brown and McQueen*, 1986] and not with the static laser-heated DAC data [*Boehler*, 1993].

[4] In order to reconcile the discrepancy in the melting temperature, another high-pressure phase with a BCC structure was proposed as a high-temperature phase of the HCP phase [*Ross et al.*, 1990; *Yoo et al.*, 1993]. In addition, a high-pressure BCC-HCP transition may be responsible for the solid-solid transition observed by *Brown and McQueen* [1986] at P = 200 GPa and T = 4400 K [*Bassett and Weathers*, 1990]. These arguments suggested that the inner core could be made of the high-pressure BCC phase. Since then, the stability of high-pressure BCC phase has been investigated only by theoretical calculations because expected P-T conditions are too extreme at present for static experiments [*Sherman*, 1994; *Stixrude et al.*, 1994; *Stixrude and Cohen*, 1995; *Soderlind et al.*, 1996; *Matsui and Anderson*, 1997; *Vočadlo et al.*, 2000; *Belonoshko et al.*, 2003; *Vočadlo et al.*, 2003], but the stability of the high-pressure BCC phase is still an open question. A recent shock wave study did not observe the solid-solid transition before melting [*Nguyen and Holmes*, 2004]. *Hemley and*

Mao [2001] proposed the melting temperature of the HCP phase will rise from the TP-2 to meet the shock wave data without introducing any other high-pressure phase. Very recently, however, from static in situ X-ray diffraction measurements in DAC experiments, *Dubrovinsky et al.* [2007] showed that a high-pressure BCC phase was stable in the $Fe_{0.9}Ni_{0.1}$ composition above P = 225 GPa and T = 3400 K.

[5] Recently, *Mikhaylushkin et al.* [2007] shed light on the stability of the FCC phase at high pressures from the first-principles calculations. They showed that the FCC-HCP transition above P = 100 GPa will be parallel to the melting curve, and the FCC phase may be stable in the inner core. They also conducted temperature-quenched laser-heated DAC experiments on pure iron above T = 3700 K at P = 160 GPa and showed the presence of a mixture of FCC + HCP phases in the temperature-quenched sample.

[6] In short, the structures of HCP, FCC, and BCC are all possible candidates in the Earth's inner core. Moreover, the estimate of the melting temperature of pure iron at the ICB varies widely from 5100 to 7100 K.

[7] One approach to resolve these issues is to construct a thermodynamic model and calculate the phase stability fields. An important point in constructing a database is that the calculated phase diagram should be consistent with the molar volume data for each phase. Reliable pressure-volume-temperature (*P-V-T*) equations of state (EoS) for iron phases are necessary for calculating a consistent phase diagram. In addition, such precise EoS are critical for estimating the amount of lighter element(s) in the core by comparison with the observed density profile (e.g., Preliminary Reference Earth Model (PREM) [*Dziewonski and Anderson*, 1981]). However, EoS for high-pressure iron phases have been a matter of debate. In particular, the unit-cell volume of the FCC phase is difficult to measure because the FCC phase is only stable at high temperature. Furthermore, the liquid volume is critically important for geophysical discussions, but is one of the least constrained parameters.

[8] In the present study, we report new *P-V-T* data of the FCC phase and develop an internally consistent thermodynamic database for pure iron phases from available thermochemical and static experimental data which include phase relations and *P-V-T* data. We have assessed the EoS for the liquid phase from the static melting data and the available density data including the Hugoniot, and we include a new calculation of the FCC melting curve. It may be hard to constrain this melting curve using first-principles calculations because of the difficulty of dealing with the magnetic effect on the energy [e.g., *Belonoshko and Ahuja*, 1997; *Mikhaylushkin et al.*, 2007]. In addition, conventional shock wave experiments cannot address FCC melting because the Hugoniot path does not go through this *P-T* region.

[9] There are existing thermodynamic data sets for pure iron based on the static experimental data [*Wood*, 1993; *Saxena and Dubrovinsky*, 1998]. These focused primarily on the calculation of phase relations (i.e., on the energy difference between phases) rather than on the integration of thermochemical and thermophysical measurements. In particular, the molar volume of the phases at high pressures was not accurately calculated in those data sets. The contribution of the volumetric term to the free energy becomes critical with increasing pressure, particularly at the Earth's core conditions. We formulated the *P-V-T* EoS of phases using the Anderson-Grüneisen parameter (δ_T) which can reliably extrapolate the thermal expansion beyond the static experimental ranges.

[10] Our study provides a comprehensive database that can be used to calculate the phase relations of iron to P = 360 GPa and T = 7000 K and addresses the issues discussed above. This database for pure iron can also serve as a reference for the development of thermodynamic models for light-element bearing iron systems.

2. Thermodynamics

[11] We calculate phase equilibrium relations based on Gibbs free energy minimization. The equilibrium of a reaction is defined by

$$\Delta G_r = 0 = \Delta H^{\circ}_{298r} + \int_{T_0}^{T} \Delta Cp^{\circ}_r dT - T\left(\Delta S^{\circ}_{298r} +\right) + \int_{P_0}^{P} \Delta V_r dP \tag{1}$$

where ΔG_r is the free energy change of the reaction, ΔH°_{298r} and ΔS°_{298r} are enthalpy and entropy changes of the reaction at a reference *P-T* condition, respectively, ΔCp°_r is the change of heat capacity of the reaction, ΔV_r is the molar volume change of the reaction at a temperature of interest, P_0 is the reference pressure, P is the pressure of interest, T_0 is the reference temperature, and T is the temperature of interest. The reference *P-T* condition in the present study is P = 1 bar and T = 298.15 K. Note that the subscript 298 which appears in parameters listed above is an abbreviation for the standard temperature of 298.15 K; this abbreviation will be used throughout this study.

[12] The change of each parameter in the reaction is calculated from $\Delta_f H^{\circ}_{298}$, the standard enthalpy of formation from the element; S°_{298}, the standard entropy; Cp°, the heat capacity; and V_0, the molar volume under reference *P-T* conditions for each of the phases included in the reaction.

[13] Heat capacity is expressed by a polynomial function as

$$Cp^{\circ} = \mathrm{a} + \mathrm{b}T + \mathrm{c}T^{-2} + \mathrm{d}T^{2} + \mathrm{e}T^{-3} + \mathrm{f}T^{-0.5} + \mathrm{g}T^{-1} \tag{2}$$

The volumetric terms are calculated from the *P-V-T* EoS of the phase. In this study, the room-temperature volume is expressed by a third-order Birch-Murnaghan EoS as

$$P_{298} = \frac{3}{2}K_0\left[\left(\frac{V_0}{V}\right)^{\frac{7}{3}} - \left(\frac{V_0}{V}\right)^{\frac{5}{3}}\right]\left\{1 - \frac{3}{4}(4 - K')*\left[\left(\frac{V_0}{V}\right)^{\frac{2}{3}} - 1\right]\right\} \tag{3}$$

where P_{298}, K_0, and K' are a pressure at T = 298.15 K, an isothermal bulk modulus, and its pressure derivative at T = 298.15 K and P = 1 bar, respectively.

[14] With the exception of the HCP phase, the thermal expansion at high pressures of all phases is evaluated by

Table 1. Unit-Cell Volume of the FCC Phase in the Work of *Komabayashi et al.* [2009]

Run	P (Obs) (GPa)	T (K)	V^a (Å^3)	P (Calc) (GPa)	ΔP (Obs-Calc) (GPa)
1st	22.1(1)	1168(8)	42.354(38)	21.7	0.4
	21.9(5)	1093(8)	42.266(39)	21.6	0.3
	20.8(2)	300(0)	41.155(63)	21.3	−0.4
2nd	29.4(3)	1309(7)	41.191(41)	29.9	−0.6
	26.2(2)	300(0)	40.563(0)	25.4	0.8
3rd	32.7(7)	1449(61)	40.911(0)	32.9	−0.2
	32.7(8)	1443(65)	40.882(10)	33.1	−0.4
	32.6(8)	1463(64)	40.960(16)	32.7	−0.1
	32.6(9)	1478(65)	40.933(18)	33.0	−0.4
	32.4(9)	1441(63)	40.942(87)	32.7	−0.3
	32.4(7)	1411(61)	40.995(0)	32.1	0.3
	32.3(7)	1383(63)	40.968(0)	32.0	0.3
	32.2(7)	1354(61)	40.944(0)	32.0	0.3
4th	44.1(1.0)	1651(64)	39.662(0)	44.0	0.1
	43.7(9)	1677(61)	39.699(0)	43.9	−0.2
	43.5(8)	1688(60)	39.736(0)	43.7	−0.2
	43.5(8)	1695(59)	39.699(0)	44.0	−0.5
	43.6(8)	1685(55)	39.709(0)	43.9	−0.3
	43.6(7)	1648(53)	39.627(0)	44.3	−0.6
5th	54.4(1.2)	1997(57)	38.698(67)	55.3	−0.8
	52.0(1.6)	2017(56)	38.715(64)	55.3	−3.3
	57.7(1.0)	2006(48)	38.647(41)	55.8	1.9
6th	65.7(1.2)	2318(104)	37.893(0)	65.9	−0.2
	67.4(1.5)	2350(123)	37.903(0)	66.1	1.3
	68.7(1.5)	2359(129)	37.866(41)	66.5	2.2
	68.2(1.9)	2377(132)	37.921(2)	66.1	2.1
	67.8(1.7)	2409(130)	37.941(10)	66.1	1.7
	65.7(1.6)	2384(124)	37.933(0)	66.0	−0.3
	64.5(1.3)	2360(130)	37.969(27)	65.4	−0.9
	63.7(2.3)	2277(119)	37.933(8)	65.2	−1.5

[a]Error zero means that the volume is calculated from a single peak.

using the Anderson-Grüneisen parameter, δ_T [*Anderson et al.*, 1992].

$$\frac{\partial \ln \alpha}{\partial \ln V} = \delta_T = \delta_0 \eta^{\kappa} \tag{4}$$

where $\eta \equiv V/V_0$, δ_0 is the value of δ_T at P = 1 bar and κ is the dimensionless thermoelastic parameter. This equation gives

$$\frac{\alpha}{\alpha_0} = \exp\left[-\frac{\delta_0}{\kappa}(1-\eta^{\kappa})\right] \tag{5}$$

where α_0 is the thermal expansivity at the reference pressure. Following *Wood* [1993], the values of δ_0 and κ are set at 6.5 and 1.4, respectively, for the FCC and BCC phases.

[15] For the HCP phase, the EoS is taken from *Dewaele et al.* [2006] which is formulated in the Mie-Grüneisen-Debye relation. As mentioned below, the thermodynamic data set is developed based on our new experimental data on the FCC-HCP transition boundary where the pressure was determined from this EoS [*Komabayashi et al.*, 2009].

[16] According to *Sundman* [1991], the magnetic contribution to the free energy (G_m) for the BCC phase is described as

$$G_m = RT\ln(\beta+1)f(\tau) \tag{6}$$

where R is the gas constant, β is the Bohr magneton number which is 2.22 for the BCC phase, τ is defined as T/T_c, and T_c is temperature of the magnetic transition which is 1043 K for the BCC phase.

[17] For $\tau < 1$,

$$f(\tau) = 1 - (1/A)\left(79\,\tau^{-1}/140p + (474/497)(1/p-1)\cdot\left(\tau^3/6 + \tau^9/135 + \tau^{15}/600\right)\right) \tag{7}$$

and for $\tau > 1$,

$$f(\tau) = -(1/A)\left(\tau^{-5}/10 + \tau^{-15}/315 + \tau^{-25}/1500\right) \tag{8}$$

where $A = (518/1125) + (11692/15975)((1/p) - 1)$ and p is a structural parameter which is 0.4 for the BCC phase [*Sundman*, 1991].

3. Data Assessment

[18] The optimized thermophysical and thermochemical parameters for all the iron phases are listed in Tables 2 and 3. We started with thermochemical data for the BCC, FCC, and liquid phases extracted from metallurgy database [*Sundman*, 1991; *Saxena and Dubrovinsky*, 1998]. We first evaluated the thermodynamic data for the FCC and HCP phases using the FCC-HCP transition boundary determined in an internally-heated diamond anvil cell experiment with an in situ X-ray diffraction method [*Komabayashi et al.*, 2009]. In this experiment, we observed cooccurrence of the FCC and HCP phases because of the sluggish kinetics, but the boundary is tightly constrained by back and forth transformations between HCP and FCC phases. We obtained *P-V-T* data of the FCC phase up to P = 69 GPa and T = 2400 K (Table 1) where the pressures were determined from the thermal EoS of the HCP phase [*Dewaele et al.*, 2006]. We adopted the 298-K EoS of the FCC phase

Table 2. Thermophysical Parameters in the Anderson-Grüneisen Equation

Phase	V_0 (cm^3 mol^{-1})	K_0 (GPa)	K'	α_0 (*10^{-5} K^{-1})	δ_0
BCC iron[a]	7.09	164	5.29	2.62 + 0.0018 * T	6.5
FCC iron[b]	6.835	165.3	5.5	6.4(1)	6.5
HCP iron[c]	6.765	165	4.97	-	-
Liquid iron[d]	6.921	124	5.77	9.2	5.22

[a]BCC iron: V_0, *Robie et al.* [1978]; K_0 and K', *Guinan and Beshers* [1968]; α_0, this study; δ_0, *Wood* [1993].

[b]FCC iron: V_0, K_0, and K', *Boehler et al.* [1990]; α_0 and δ_0, this study.

[c]HCP iron: all parameters from *Dewaele et al.* [2006]. Vibrational, anharmonic, and electronic thermal pressure effects are added to the 300 K pressure. See *Dewaele et al.* [2006] for details.

[d]Liquid iron: V_0, K_0, and K', this study; α_0, *Anderson and Ahrens* [1994]; δ_0, this study.

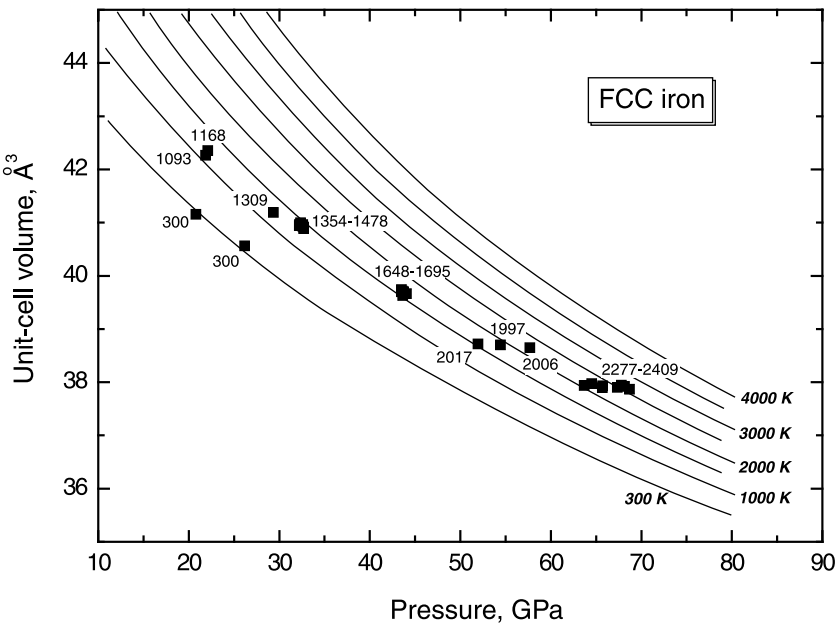

Figure 2. Calculated isothermal compression curves of the FCC phase at $T = 300$ K and 1000 to 4000 K with 500 K intervals. Symbols are from recent internally-heated DAC experiments [*Komabayashi et al.*, 2009]. Numbers attached to the symbols are the experimental temperatures. Fitted parameters are listed in Table 2.

from *Boehler et al.* [1990] with V_0, K_0, and K' of 6.835 cm^3 mol^{-1}, 165.3 GPa, and 5.5, respectively. Fitting our *P-V-T* data to the Anderson-Grüneisen relation yielded α_0 of 6.4 ± 0.1 (2σ) × 10^{-5} K^{-1}. The optimized parameters are listed in Table 2, and the calculated isothermal compression curves are shown in Figure 2.

[19] For the HCP phase, the EoS is from *Dewaele et al.* [2006]. Thermochemistry for this phase is not available since this phase is not quenchable to the ambient condition. We assume that $Cp°$ for the HCP phase at P = 1 bar is identical to $Cp°$ for the FCC phase up to $T = 7000$ K based on their similar Debye temperature (335 K for the FCC phase [*Zarestky and Stassis*, 1987] and 417 K for the HCP phase [*Dewaele et al.*, 2006]). A calculation of $Cp°$ for the HCP phase from the *Dewaele et al.*'s [2006] EoS up to T = 900 K differed less than 2% from $Cp°$ values for the FCC phase, supporting our assumption. The $\Delta_f H°_{298}$ and $S°_{298}$ were evaluated from the *P-T* locations of the FCC-HCP boundary, with values of 5945 J mol^{-1} and 32.4 J mol^{-1} K^{-1}, respectively. (Table 3)

[20] For the liquid phase, thermochemical parameters were taken from metallurgy data. The volume-temperature relationship at $P = 1$ bar is taken from *Anderson and Ahrens* [1994]. The volume at the ambient pressure melting temperature ($T = 1811$ K) and thermal expansivity were fixed at 7.957 cm^3 mol^{-1} and 9.20 × 10^{-5} K^{-1}, respectively. The remaining EoS parameters were estimated from the experimentally determined FCC and HCP melting curves up to P = 200 GPa [*Shen et al.*, 1998; *Boehler et al.*, 1990; *Boehler*, 1993]. The K_0, K', and δ_0 were determined to be 124 GPa, 5.77, and 5.22, respectively, with κ fixed at 1.4. The density of the liquid phase and its effect on iron melting curves will be discussed in more detail below.

[21] For the low-pressure BCC phase, thermochemistry including a magnetic contribution is from the metallurgy data [*Sundman*, 1991; *Saxena and Dubrovinsky*, 1998]. The EoS was assessed from the literature [*Guinan and Beshers*, 1968; *Boehler and Ramakrishnan*, 1980]. Note that BCC phase EoS parameters were previously reported in terms of Mie-Grüneisen theory [*Boehler and Ramakrishnan*, 1980].

Table 3. Thermochemical Parameters[a]

Phase[b]	a	b	c	d	e	f	ext
BCC iron (298.15 < T < 1811 K)	1400	124.06	−23.5143	−0.00439752	−5.8927E−08	77359	0
BCC iron (1811 < T < 7000 K)	−25383.581	299.31255	−46	0	0	0	2.29603E+31 * T^{-9}
FCC iron (298.15 < T < 7000 K)	16300.921	381.47162	−52.2754	0.000177578	0	−395355.43	−2476.28 * $T^{0.5}$
HCP iron[c] (298.15 < T < 7000 K)	14405.9211	384.8716162	−52.2754	0.000177578	0	−395355.43	−2476.28 * $T^{0.5}$
Liquid (1811 < T < 7000K)	−9007.3402	290.29866	−46	0	0	0	0

[a]Gibbs energy at 1 bar, J·mol^{-1} = a + bT + cTln$T$ + dT^2 + eT^3 + fT^{-1} + ext.
[b]For all the phases except for HCP iron, the parameters were assessed by *Saxena and Dubrovinsky* [1998].
[c]For HCP iron, standard enthalpy of formation and standard entropy were assessed in this study. Heat capacity was assumed to be same as FCC iron.

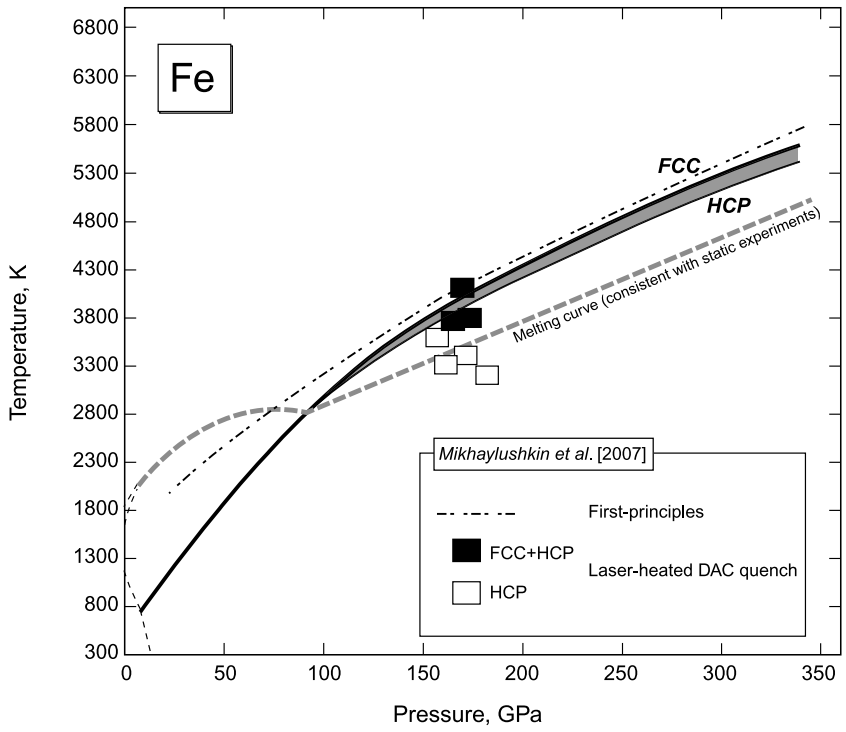

Figure 3. Calculated FCC-HCP phase transition boundary (this study) together with the melting curve (this study) shown by the thick dashed line (taken from Figure 5). The grey field corresponds to the uncertainty in the location of the phase boundary due to uncertainties in the fitting of the EoS for the FCC phase. The transition boundary with the best-fitted parameters for the EoS for the FCC phase is shown as the thick solid line. Note that the best-fit curve is not necessarily at the middle of the grey range since ΔH°_{298r} and ΔS°_{298r} were changed according to the error in the elastic parameter. Results from first-principles calculations and temperature-quenched laser-heated DAC experiments by *Mikhaylushkin et al.* [2007] are also plotted. Above P = 150 GPa, the first-principles calculations and our thermodynamic calculations are consistent. The experiments by *Mikhaylushkin et al.* [2007] were made in the liquid stability field according to our calculation of the melting curve.

In this study, however, the EoS was reformulated in the Anderson-Grüneisen relations for simplicity. In addition, a single EoS was used for both low-T magnetic BCC (α phase) and high-T non-magnetic BCC phase (δ phase). Nonmagnetic phases are likely to have different physical parameters due to the different spin state. However, this is not significant for stability calculations over a narrow P-T range (to P = 5 GPa and T = 2000 K).

4. Results and Discussion

4.1. FCC-HCP Transition Boundary

[22] Figure 3 shows the calculated FCC-HCP boundary to the inner core boundary pressure (P = 330 GPa) together with the melting curve constrained by the static laser-heated DAC data (the thick grey dashed line). The plotted uncertainty in the position of the boundary reflects the uncertainty in the EoS of the FCC phase (Table 2). The HCP-FCC-liquid triple point (TP-2) is located at P = 90 GPa and T = 2800 K. Our calculations constrain the extent of the curvature of the FCC-HCP transition boundary in the melt stability field from P = 100 to 150 GPa. At higher pressure, the boundary is almost parallel to the static experimental data of HCP-liquid curve. This curvature is due to the difference in the thermoelastic parameters between the HCP and FCC phases. The best-fit FCC-HCP transition boundary remains above the melting curve beyond the FCC-HCP-liquid triple point (TP-2), implying that the HCP phase is stable below the melting temperatures constrained by static laser-heated DAC data over the entire core pressure range (Figure 3). Above P = 150 GPa, our calculated FCC-HCP boundary is in good agreement with recent theoretical calculations by *Mikhaylushkin et al.* [2007]. *Mikhaylushkin et al.* [2007] also conducted temperature-quenched laser-heated DAC experiments and observed a FCC + HCP mixture in the sample quenched from T = 3700 K at P = 160 GPa. They discussed the possibility of the FCC phase being stable below the melting curve at high pressures. However, the temperatures where the FCC phase was observed in the quenched sample were above the melting curve of iron [*Boehler*, 1993]. In addition, our calculations show that the Gibbs free energy of the liquid phase is smaller than that of the FCC phase at all temperature up to P = 330 GPa (Figure 4). Therefore, the FCC phase is unlikely to be stabilized below the HCP melting temperatures. It is possible that the FCC phase observed in the experiments of *Mikhaylushkin et al.* [2007] is quenched as a metastable phase from temperatures above the melting point.

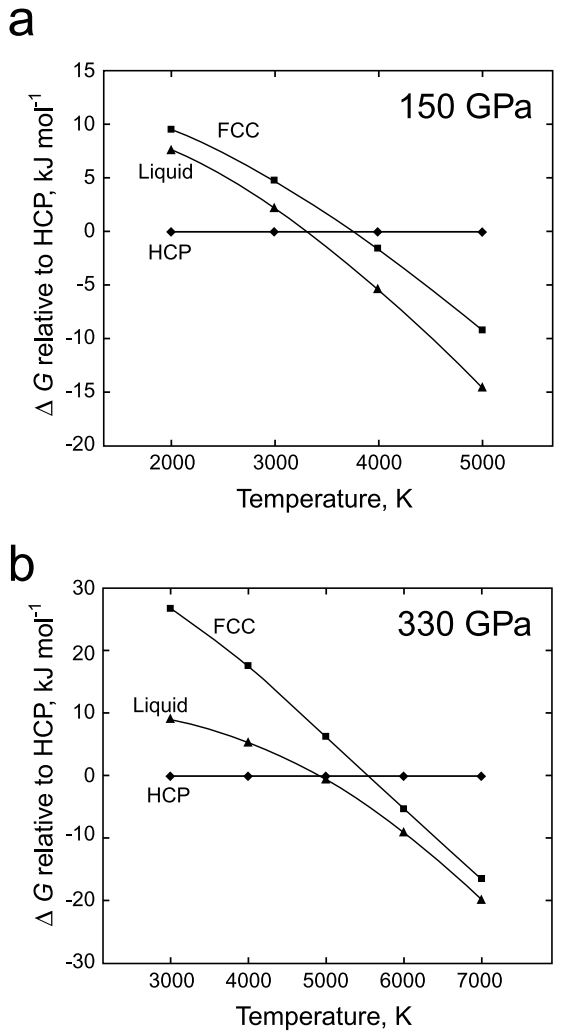

Figure 4. Gibbs free energies of the HCP, FCC, and liquid phases relative to that of the HCP phase as a function of temperature at (a) P = 150 GPa and (b) P = 330 GPa. The Gibbs free energy of the FCC phase is always higher than that of the liquid phase. FCC, face-centered cubic phase; HCP, hexagonal close-packed phase.

4.2. Iron Melting Curve

[23] The P-T location and Clayperon slope of the HCP iron melting curve are critical for estimating the temperature of the inner core boundary at P = 330 GPa. However, the P-V-T EoS for liquid iron is poorly constrained. In this section we explore the effect of the liquid EoS on the resulting melting curves of the FCC and HCP phases. Figure 5 shows the calculated phase relations for iron to P = 360 GPa with two different EoS for the liquid phase, compared with the experimental data [*Brown and McQueen*, 1986; *Boehler et al.*, 1990; *Yoo et al.*, 1993; *Boehler*, 1993; *Shen et al.*, 1998; *Nguyen and Holmes*, 2004; *Komabayashi et al.*, 2009]. Figure 6 shows the density of the liquid phase from each EoS at T = 5000 K and 6000 K, compared with the density profile for the Earth's core from PREM [*Dziewonski and Anderson*, 1981].

[24] *Anderson and Ahrens* [1994] proposed an EoS for the liquid phase based on melt density data at P = 1 bar [*Lucas*, 1972; *Drotning*, 1981], 0.2 GPa [*Hixson et al.*, 1990], and along the Hugoniot [*Al'tshuler et al.*, 1958, 1962; *Krupnikov et al.*, 1963; *Marsh*, 1980; *Al'tshuler et al.*, 1981]. The calculated melting curve of FCC iron based on these data is shown in Figure 5. The curve reaches unrealistically high temperatures at P = 100 GPa, suggesting this EoS does not accurately represent density of liquid iron at that pressure. The result indicates that the liquid density is too small at low pressures and high temperature, as shown in Figure 6. The failure of this EoS is likely due to lack of constraints on liquid density data from P = 0.2 GPa to the Hugoniot pressures (∼240 GPa). Therefore, we chose to use the phase equilibrium data to put constraints on the EoS for the liquid. Note that very few first-principles calculations were made on FCC melting due to the difficulty of dealing with the magnetic effect on FCC energy [e.g., *Belonoshko and Ahuja*, 1997; *Mikhaylushkin et al.*, 2007].

[25] To constrain the EoS of liquid iron, we used the density data at P = 1 bar [*Lucas*, 1972; *Drotning*, 1981], 0.2 GPa [*Hixson et al.*, 1990], and along the Hugoniot [*Brown and McQueen*, 1986], as well as the melting temperatures obtained from the laser-heated DAC experiments [*Shen et al.*, 1998; *Boehler et al.*, 1990; *Boehler*, 1993]. The calculated melting curve is shown in Figure 5. In constructing the liquid EoS, the misfit to the Hugoniot data above P = 280 GPa and T = 6600 K is 5.0−5.2% in pressure, which we consider acceptable. Thus, we obtained the phase diagram which is consistent with the static DAC data and the Hugoniot density data. The melting temperature at P = 330 GPa is 4900 K, and the density change on melting is −1.2%.

[26] The above analysis illustrates that density data between P = 0.2 GPa and in the Hugoniot are critical to calculate the melting curve of iron. The density data in this pressure range provide a tight constraint on the FCC melting curve. Figure 3 demonstrated that the FCC-HCP transition boundary is curved at high-P-T conditions, and therefore, the FCC phase will have a wider stability than previously thought, if the FCC melting temperature is very high. The melting curve of the FCC iron up to 60 GPa has not been controversial in the static DAC experiments [*Shen et al.*, 1998; *Boehler et al.*, 1990]. Therefore the FCC melting temperature can be used as a critical constraint in constructing EoS for iron liquid. Thus, our fit is chosen as a primary result in this study since it reproduces the melting curve of the FCC phase. However, our fit cannot reproduce the shock wave melting points, although it is consistent with the Hugoniot density data for liquid iron. This indicates that the discrepancies between the shock wave and static data are not in the liquid density but in the equilibrium melting temperature.

[27] We superimposed the liquid density curve by *Alfè et al.* [2000] at T = 6000 K in Figure 6 for comparison. The density curve of *Alfè et al.* [2000] is in good agreement with our curve. However, the melting temperature of the HCP phase of *Alfè et al.* [1999] is very high (Figure 1). The difference in the melting temperature of the HCP phase between *Alfè et al.* [1999] and this study may be related to the difference in the entropy of the melting.

[28] At the melting temperature of the HCP phase of 4900 K at P = 330 GPa, we calculated the Earth's core density deficit by comparing the PREM density with the

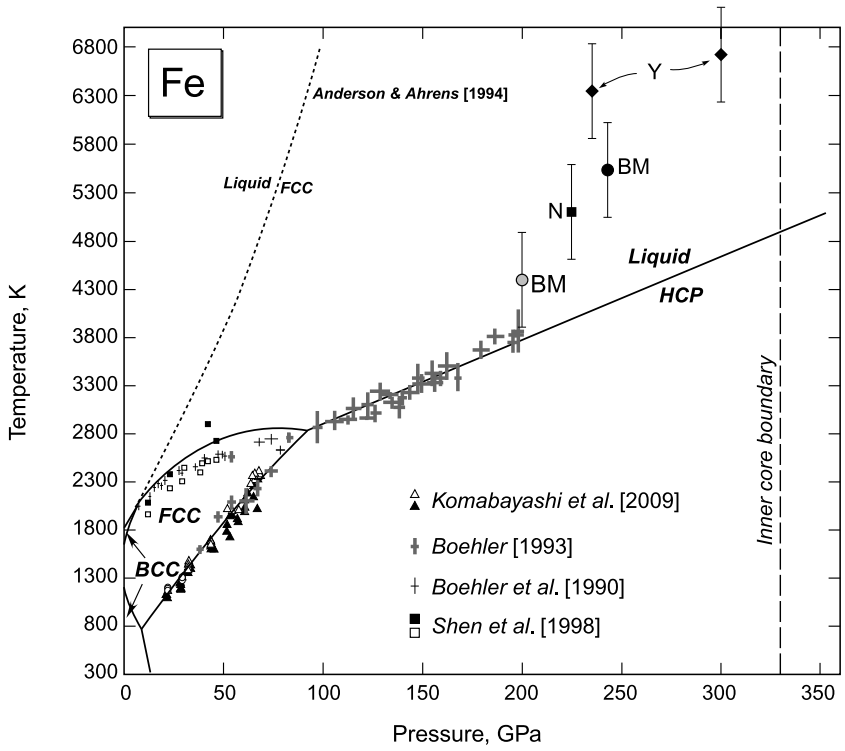

Figure 5. Calculated phase relations of pure iron (solid lines, this study) together with existing static experimental data (symbols, from *Boehler et al.* [1990], *Boehler* [1993], *Shen et al.* [1998], and *Komabayashi et al.* [2009]). The melting curves were calculated with the EoS of the liquid phase by *Anderson and Ahrens* [1994] (dashed line) and this study (solid line). The EoS by *Anderson and Ahrens* [1994] is based on existing density data, while that in this study is assessed from existing density data as well as melting experiments in the laser-heated DAC. The shock wave data (black, melting; grey, solid-solid reaction) are also plotted: BM, *Brown and McQueen* [1986]; Y, *Yoo et al.* [1993]; N, *Nguyen and Holmes* [2004]. BCC, body-centered cubic phase; FCC, face-centered cubic phase; HCP, hexagonal close-packed phase.

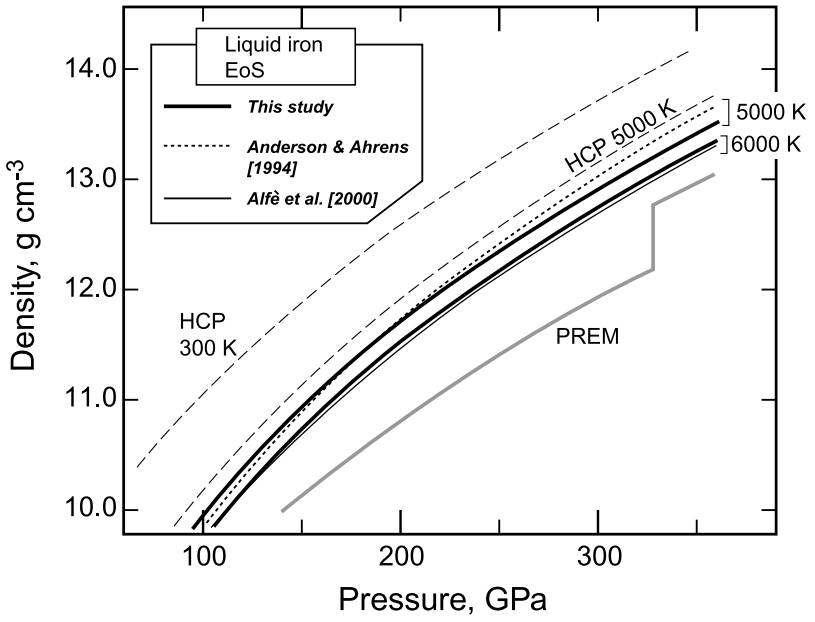

Figure 6. High-temperature isothermal density curves of the HCP and liquid phase together with the PREM density data [*Dziewonski and Anderson*, 1981]. The curve of the HCP phase is from *Dewaele et al.* [2006]. The liquid curves are from *Anderson and Ahrens* [1994], *Alfè et al.* [2000], and this study.

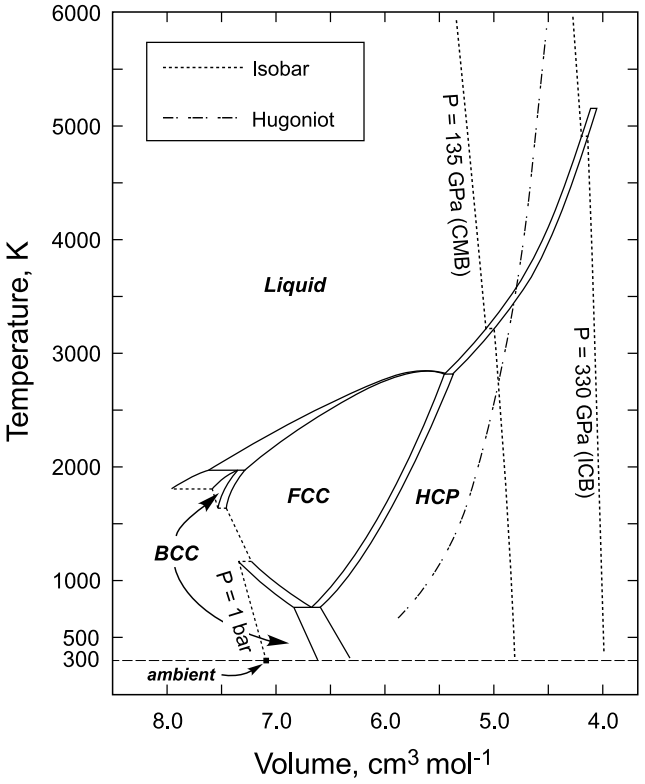

Figure 7. Stability diagram in molar volume-temperature space assuming there is no post-HCP solid iron phase. Isobars and Hugoniot path [*Brown and McQueen*, 1986] are shown. CMB, core-mantle boundary; ICB, inner core boundary.

density of liquid (liquid outer core side) and of HCP iron (solid inner core side). The calculated core density deficits at the inner core boundary are 8.1 wt.% and 5.3 wt.% for the liquid outer core and solid inner core, respectively. The core density deficit would be smaller for higher core temperatures.

[29] Figure 7 shows the Fe phase diagram in molar volume-temperature space (i.e., using the Helmholtz free energy). The present calculations precisely describe the molar volume (density) change at each phase transition. Compared to previous estimates [*Anderson and Isaak*, 2000], the volume change at the FCC-HCP transition is smaller by approximately 50 per cent in this study. This volume change was directly determined by our in situ X-ray diffraction measurements [*Komabayashi et al.*, 2009], providing a better constraint compared to the previous estimates.

4.3. Stability of a High-Pressure BCC Phase and Its Implications for the Earth's Core

[30] The calculated phase relations (Figure 5), partly derived from static high-pressure experiments, show that the melting temperature of HCP iron at the ICB (P = 330 GPa) is 4900 K, which is much lower than the melting temperature at this pressure derived from a series of shock wave experiments [*Brown and McQueen*, 1986; *Yoo et al.*, 1993; *Nguyen and Holmes*, 2004]. As discussed above, it is possible to reproduce the static melting data of the HCP phase using liquid density data obtained from shock wave experiments [*Brown and McQueen*, 1986]. Therefore, the discrepancy between the static and shock wave studies is related to the equilibrium melting temperature. *Hemley and Mao* [2001] suggested that if the FCC-HCP-liquid triple point (TP-2) is located at P = 60 GPa [*Shen et al.*, 1998], the melting curve for the HCP phase may reach the shock wave melting temperature at P = 300 GPa. However, recent in situ measurements showed that the FCC-HCP boundary has a steeper dP/dT slope which moves the TP-2 to P = 88 GPa and T = 2800 K [*Komabayashi et al.*, 2009]. In constructing the present phase diagram, we used experimental data of *Komabayashi et al.* [2009] for the FCC-HCP transition boundary which was determined by in situ X-ray diffraction measurements in the internally-heated diamond-anvil cell with pressures determined from the unit-cell volume of HCP iron based on its EoS proposed by *Dewaele et al.* [2006]. The boundary is also consistent with the multi-anvil experimental results by *Kubo et al.* [2003] who determined the boundary using MgO as the internal pressure standard. Magnesium oxide is the least controversial pressure standard to date. The calculated HCP melting curve, based on consistent EoS of iron phases and the melting curve of FCC iron, gives relatively low melting temperatures (Figure 5) that cannot match the high shock wave melting temperature.

[31] An alternative explanation for the shock-wave derived high melting temperatures is the presence of another high-P-T phase (post-HCP phase) stable at pressures above 200 GPa, not covered by static high-pressure experiments. Several shock wave studies have suggested the existence of a solid-solid transition at P = 200 GPa before melting in the Hugoniot [*Brown and McQueen*, 1986; *Brown*, 2001], although *Nguyen and Holmes* [2004] did not observe such a transition. According to theoretical calculations, the FCC phase may be stabilized at high pressure [*Mikhaylushkin et al.*, 2007], although the thermodynamic analysis of this study shows that the FCC phase is unlikely to be stabilized at high pressures (Figures 3 and 4).

[32] *Bassett and Weathers* [1990] discussed the possible presence of a high-pressure BCC phase. A key issue was whether or not the metastable extension of the BCC (δ phase)-FCC transition has a curvature at higher P-T regions. If it does, the BCC-FCC reaction crosses the melting curve at higher pressure, introducing a high-pressure BCC phase as a high-temperature phase of the HCP phase. If the high-pressure BCC phase is stable, high-P BCC-HCP transition can explain the solid-solid transition, and the BCC phase may have a high melting temperature. Subsequently, *Stixrude and Cohen* [1995] dismissed this possibility on the basis of first-principles calculations showing the energy of BCC iron would be much higher than that of the HCP and FCC solid phases at high pressures. On the other hand, *Dubrovinsky et al.* [2007] recently reported a high-pressure BCC iron phase with 10% Ni at P = 225 GPa and T = 3400 K, based on in situ X-ray diffraction measurements in static DAC experiments.

[33] In Figure 8 we present a Schreinemakers analysis on the topology of the Fe phase diagram, including BCC reactions, where the BCC phase is restabilized at the TP-5. Note that Figure 8 shows topological relationships only, where the detail P-T values are not significant. For this topology to be achieved, as *Bassett and Weathers* [1990] discussed, elastic parameters should be different between the BCC and other phases. If K' for the BCC phase is lower

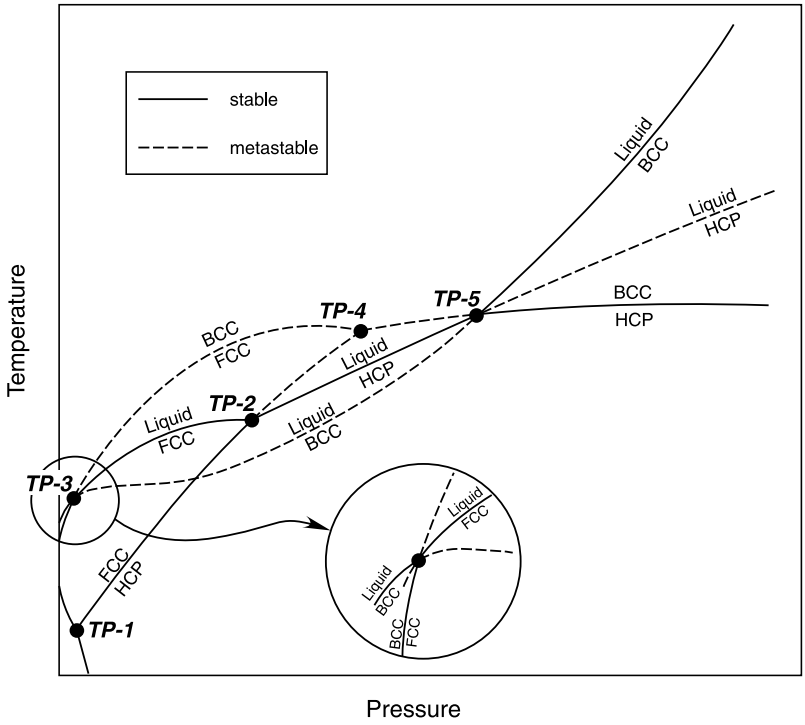

Figure 8. Schreinemakers analysis of the low-pressure BCC phase being restabilized at high pressures. From the metastable invariant point of FCC, BCC, and HCP (TP-4), a new reaction between the HCP and high-*P* BCC phase originates toward high pressure. However, the metastable melting curve of the BCC phase has two turning points from the TP-3 to TP-5 before it is restabilized as a high-*P* BCC melting curve, which is physically unreasonable.

than for the other phases, the metastable BCC-FCC boundary will be bending down with increasing pressure from TP-3 to TP-4. The metastable FCC-BCC transition will cross the metastable FCC-HCP transition at high pressures, to form another invariant point (TP-4). From TP-4, high-*P* BCC-HCP transition originates toward high pressure, stabilizing high-*P* BCC phase as a high-temperature phase of the HCP phase. However, the low-*P* BCC-melt curve also has a metastable *P*-*T* evolution. It comes in as a stable reaction when high-*P* BCC is stabilized at the TP-5. This BCC-melt curve has at least two turning points from the TP-3 to TP-5, which is physically unreasonable. In addition, the melting curve of the high-*P* BCC phase is concave downward, which is also physically unreasonable for the melting phenomenon. Thus, the scenario that the low-*P* BCC phase is restabilized at high pressures is abandoned on the basis of the topological arguments.

[34] Another alternative scenario was proposed by *Belonoshko et al.* [2003], on the basis of first principles calculations, namely that a high-*P* BCC phase different from the low-*P* BCC phase is stabilized above P = 105 GPa and T = 3300 K. Subsequently, the EoS for this high-*P* BCC phase was reported [*Belonoshko et al.*, 2008]. Comparison of the HCP phase [*Dewaele et al.*, 2006] with the high-*P* BCC phase [*Belonoshko et al.*, 2008] showed that the BCC phase's energy has a weaker temperature dependence, indicating that the BCC phase of *Belonoshko et al.* [2008] cannot be stabilized as the high temperature phase of the HCP iron of *Dewaele et al.* [2006]. Here we try to include *Belonoshko et al.*'s [2008] BCC phase into our database. We adopted the EoS by *Belonoshko et al.* [2008] for the high-*P* BCC phase. We assumed the thermochemical properties of the high-*P* BCC phase so that (1) the high-*P* BCC-HCP boundary is located at P = 220 GPa and T = 3900 K which is inferred in the shock wave experiments [*Brown and McQueen*, 1986] and (2) the melting temperature of the high-*P* BCC phase is close to the shock wave melting temperatures [*Brown and McQueen*, 1986; *Yoo et al.*, 1993; *Nguyen and Holmes*, 2004]. The heat capacity at P = 1 bar for the high-*P* BCC phase was assumed to be the same as for the low-*P* BCC phase. For the $\Delta_f H^\circ_{298}$ and S°_{298} of the high-*P* BCC phase, 28 kJ mol^{-1} and -6 J mol^{-1} K^{-1} were added, respectively, to those of the low-*P* BCC phase. Thus the hypothetical high-*P* BCC phase has different thermodynamic properties from the low-*P* BCC phase. Although the inclusion of the high-*P* BCC may be not well justified until confirmation of such a phase, this calculation gives insightful information about high-*P* BCC phase stability. The results are shown in Figure 9. The high-*P* BCC phase is stabilized as a high-temperature phase of the HCP phase due to larger temperature dependence of the free energy (i.e., the entropy of the BCC phase of this study is larger than that of *Belonoshko et al.*'s [2008] BCC phase). Depending on the entropy of the BCC phase, the melting temperature can meet the shock wave values (Figure 9). Note that we do not claim that Figure 9 is quantitatively correct. However, in order to reconcile the static and shock wave experimental data, a putative high-*P*-*T* iron solid

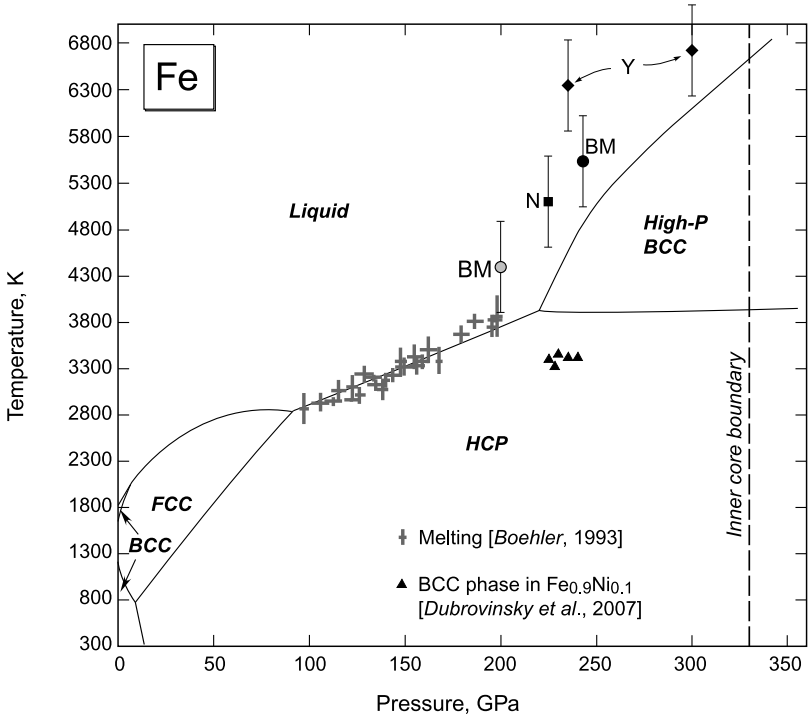

Figure 9. Iron phase diagram including a hypothetical high-*P* BCC phase. The EoS for high-*P* BCC phase is taken from *Belonoshko et al.* [2008], while the thermochemical parameters were assessed in this study so that the phase relations can explain the shock wave experimental data. If the entropy of the BCC phase is large compared with that of the HCP phase, the melting temperature will be increased. This diagram is not quantitative, just for the discussion of the BCC phase properties if it exists.

phase should have a large entropy. As discussed above, our analyses clearly showed that neither the HCP nor FCC phase can explain the shock wave melting temperatures. The high-pressure BCC phase on the other hand has the potential to reconcile the discrepancies between shock wave and static experiments. Further experiments under inner core pressure-temperature conditions are required to confirm the existence of this BCC phase.

[35] **Acknowledgments.** This research was supported by NASA and NSF grants to YF (NNX07AF94G and EAR-0809539), by the Carnegie Institution of Washington, and by the Grant-in-Aid for Young Scientists (B) to T.K. (20740306) from the Ministry of Education, Culture, Sports, Science and Technology, Japan. Constructive and insightful reviews by A. Belonoshko, M. Jacobs, and L. Dubrovinsky have greatly improved the manuscript. We thank the Associate Editor, W. van Westrenen for his suggestions on the manuscript at the final stage.

References

Alfè, D., M. J. Gillan, and G. D. Price (1999), The melting curve of iron at the pressures of the Earth's core from ab initio calculations, *Nature*, *401*, 462–464, doi:10.1038/46758.

Alfè, D., G. Kresse, and M. J. Gillan (2000), Structure and dynamics of liquid iron under Earth's core conditions, *Phys. Rev. B*, *61*, 132–142, doi:10.1103/PhysRevB.61.132.

Al'tshuler, L. V., K. K. Krupnikov, B. N. Ledenev, V. I. Zhuchikhin, and M. I. Brozhnik (1958), Dynamic compressibility and equation of state of iron under high pressure, *Sov. Phys. JETP Engl. Transl.*, *34*(7), 606–619.

Al'tshuler, L. V., A. A. Bakanova, and R. F. Trunin (1962), Shock adiabats and zero isotherms of seven metals at high pressures, *Sov. Phys. JETP Engl. Transl.*, *15*, 65–74.

Al'tshuler, L. V., A. A. Bakanova, I. P. Dudoladov, E. A. Dynin, R. F. Trunin, and B. S. Chekin (1981), Shock adiabatic curves of metals: New data, statistical analysis, and general laws, *J. Appl. Mech. Tech. Phys. Engl. Transl.*, *22*, 141–169.

Anderson, O. L. (1995), *Equations of State of Solids for Geophysics and Ceramic Science*, 405 pp., Oxford Univ. Press, New York.

Anderson, O. L., and D. G. Isaak (2000), Calculated melting curves for phases of iron, *Am. Mineral.*, *85*, 376–385.

Anderson, O. L., H. Oda, and D. G. Isaak (1992), A model for the computation of thermal expansivity at high compression and high temperatures: MgO as an example, *Geophys. Res. Lett.*, *19*(19), 1987–1990, doi:10.1029/92GL02145.

Anderson, W. W., and T. J. Ahrens (1994), An equation of state for liquid iron and implications for the Earth's core, *J. Geophys. Res.*, *99*(B3), 4273–4284, doi:10.1029/93JB03158.

Andrault, D., G. Fiquet, M. Kunz, F. Visocekas, and D. Haeusermann (1997), The orthorhombic structure of iron: An in situ study at high-temperature and high-pressure, *Science*, *278*, 831–834, doi:10.1126/science.278.5339.831.

Bassett, W. A., and M. S. Weathers (1990), Stability of the body-centered cubic phase of iron: A thermodynamic analysis, *J. Geophys. Res.*, *95*(B13), 21,709–21,711, doi:10.1029/JB095iB13p21709.

Belonoshko, A. B., and R. Ahuja (1997), Embedded-atom molecular dynamics study of iron melting, *Phys. Earth Planet. Inter.*, *102*, 171–184, doi:10.1016/S0031-9201(97)00014-9.

Belonoshko, A. B., R. Ahuja, and B. Johansson (2000), Quasi-ab initio molecular dynamics study of Fe melting, *Phys. Rev. Lett.*, *84*(16), 3638–3641, doi:10.1103/PhysRevLett.84.3638.

Belonoshko, A. B., R. Ahuja, and B. Johansson (2003), Stability of the body-centered-cubic phase of iron in the Earth's inner core, *Nature*, *424*, 1032–1034, doi:10.1038/nature01954.

Belonoshko, A. B., P. I. Dorogokupets, B. Johansson, S. K. Saxena, and L. Koci (2008), Ab initio equation of state for the body-centered-cubic phase of iron at high pressure and temperature, *Phys. Rev. B*, *78*, 104107, doi:10.1103/PhysRevB.78.104107.

Boehler, R. (1993), Temperatures in the Earth's core from melting-point measurements of iron at high static pressures, *Nature*, *363*, 534–536, doi:10.1038/363534a0.

Boehler, R., and J. Ramakrishnan (1980), Experimental results on the pressure dependence of the Gruneisen parameter: A review, *J. Geophys. Res.*, *85*(B12), 6996–7002, doi:10.1029/JB085iB12p06996.

Boehler, R., N. von Bargen, and A. Chopelas (1990), Melting, thermal expansion, and phase transitions of iron at high pressures, *J. Geophys. Res.*, *95*(B13), 21,731–21,736, doi:10.1029/JB095iB13p21731.

Brown, J. M. (2001), The equation of state of iron to 450 GPa: Another high pressure solid phase?, *Geophys. Res. Lett.*, *28*(22), 4339–4342, doi:10.1029/2001GL013759.

Brown, M. J., and R. G. McQueen (1986), Phase transitions, Grüneisen parameter, and elasticity for shocked iron between 77 GPa and 400 GPa, *J. Geophys. Res.*, *91*(B7), 7485–7494, doi:10.1029/JB091iB07p07485.

Dewaele, A., P. Loubeyre, F. Occelli, M. Mezouar, P. I. Dorogokupets, and M. Torrent (2006), Quasihydrostatic equation of state of iron above 2 Mbar, *Phys. Rev. Lett.*, *97*, 215504, doi:10.1103/PhysRevLett.97.215504.

Drotning, W. D. (1981), Thermal expansion of iron, cobalt, nickel, and copper at temperatures to 600 K above melting, *High Temp. High Pressures*, *13*, 441–458.

Dubrovinsky, L., et al. (2007), Body-centered cubic iron-nickel alloy in Earth's core, *Science*, *316*, 1880–1883, doi:10.1126/science.1142105.

Dziewonski, A. M., and D. L. Anderson (1981), Preliminary reference Earth model, *Phys. Earth Planet. Inter.*, *25*, 297–356, doi:10.1016/0031-9201(81)90046-7.

Gilvarry, J. J. (1956), The Lindemann and Gruneisen laws, *Phys. Rev.*, *102*, 307–316.

Guinan, M. W., and D. N. Beshers (1968), Pressure derivatives of the elastic constants of α-iron to 10 kbs, *J. Phys. Chem. Solids*, *29*, 541–549, doi:10.1016/0022-3697(68)90131-5.

Hemley, R. J., and H. K. Mao (2001), In situ studies of iron under pressure: New windows on the Earth's core, *Int. Geol. Rev.*, *43*, 1–26.

Hixson, R. S., M. A. Winkler, and M. L. Hodgdon (1990), Sound speed and thermophysical properties of iron and nickel, *Phys. Rev. B*, *42*, 6485–6491, doi:10.1103/PhysRevB.42.6485.

Komabayashi, T., Y. Fei, Y. Meng, and V. Prakapenka (2009), In-situ X-ray diffraction measurements of the γ-ε transition boundary of iron in an internally-heated diamond anvil cell, *Earth Planet. Sci. Lett.*, *282*, 252–257, doi:10.1016/j.epsl.2009.03.025.

Krupnikov, K. K., A. A. Bakanova, M. I. Brazhnik, and R. F. Trunin (1963), An investigation of the shock compressibility of titanium, molybdenum, tantalum, and iron, *Sov. Phys. Dokl., Engl. Transl.*, *8*, 205–207.

Kubo, A., E. Ito, T. Katsura, T. Shinmei, H. Yamada, O. Nishikawa, M. Song, and K. Funakoshi (2003), In situ x-ray observation of iron using Kawai-type apparatus equipped with sintered diamond: absence of β phase up to 44 GPa and 2100 K, *Geophys. Res. Lett.*, *30*(3), 1126, doi:10.1029/2002GL016394.

Laio, A., S. Bernard, G. L. Chiarotti, S. Scandolo, and E. Tosatti (2000), Physics of iron at Earth's core conditions, *Science*, *287*, 1027–1030, doi:10.1126/science.287.5455.1027.

Li, J., and Y. Fei (2007), Experimental constraints on core composition, in *Treatise on Geochemistry Update*, edited by H. D. Holland and K. K. Turekian, pp. 1–31, Elsevier, New York.

Lucas, L. D. (1972), Densite de metaux a haute temperature (dans les etats solide et liquide), *Mem. Sci. Rev. Metall.*, *69*, 479–492.

Ma, Y., M. Somayazulu, G. Shen, H.-K. Mao, J. Shu, and R. J. Hemley (2004), In situ X-ray diffraction studies of iron to Earth-core conditions, *Phys. Earth Planet. Inter.*, *143–144*, 455–467, doi:10.1016/j.pepi.2003.06.005.

Marsh, S. P. (1980), *LASL Shock Hugoniot Data*, 658 pp., Univ. of Calif. Press, Berkeley.

Matsui, M., and O. L. Anderson (1997), The case for a body-centered cubic phase (α') for iron at inner core conditions, *Phys. Earth Planet. Inter.*, *103*, 55–62, doi:10.1016/S0031-9201(97)00020-4.

Mikhaylushkin, A. S., S. I. Simak, L. S. Dubrovinsky, N. A. Dubrovinskaia, B. Johansson, and I. A. Abrikosov (2007), Pure iron compressed and heated to extreme conditions, *Phys. Rev. Lett.*, *99*, 165505, doi:10.1103/PhysRevLett.99.165505.

Nguyen, J. H., and N. C. Holmes (2004), Melting of iron at the physical conditions of the Earth's core, *Nature*, *427*, 339–342, doi:10.1038/nature02248.

Robie, R. A., B. S. Hemingway, and J. R. Fisher (1978), Thermodynamic properties of minerals and related substances at 298.15 K and 1 Bar (10^5 pascals) pressure and at higher temperatures, 456 pp., U.S. Geol. Surv. Bull., Washington, D. C.

Ross, M., D. A. Young, and R. Grover (1990), Theory of the iron phase diagram at Earth core conditions, *J. Geophys. Res.*, *95*(B13), 21,713–21,716, doi:10.1029/JB095iB13p21713.

Saxena, S. K., and L. S. Dubrovinsky (1998), Thermodynamics of iron phases at high pressures and temperatures, in *Properties of Earth and Planetary Materials*, edited by M. H. Manghnani and T. Yagi, pp. 271–279, AGU, Washington, D. C.

Saxena, S. K., and L. S. Dubrovinsky (2000), Iron phases at high pressures and temperatures: phase transition and melting, *Am. Mineral.*, *85*, 372–375.

Saxena, S. K., L. S. Dubrovinsky, P. Haeggkvist, Y. Cerenius, G. Shen, and H. K. Mao (1995), Synchrotron x-ray study of iron at high pressure and temperature, *Science*, *269*, 1703–1704, doi:10.1126/science.269.5231.1703.

Shen, G., H.-K. Mao, R. J. Hemley, T. S. Duffy, and M. L. Rivers (1998), Melting and crystal structure of iron at high pressures and temperatures, *Geophys. Res. Lett.*, *25*(3), 373–376, doi:10.1029/97GL03776.

Sherman, D. J. (1994), Electronic structure, entropy and the high-pressure stability of BCC iron, in *High Pressure Science and Technology-1993*, edited by S. C. Schmidt et al., pp. 895–898, Am. Phys. Soc., New York.

Soderlind, P., J. A. Moriarty, and J. M. Wills (1996), First-principles theory of iron up to earth-core pressures: structural, vibrational, and elastic properties, *Phys. Rev. B*, *53*(21), 14,063–14,072, doi:10.1103/PhysRevB.53.14063.

Stixrude, L., and R. E. Cohen (1995), Constraints on the crystalline structure of the inner core: mechanical instability of BCC iron at high pressure, *Geophys. Res. Lett.*, *22*(2), 125–128, doi:10.1029/94GL02742.

Stixrude, L., R. E. Cohen, and D. J. Singh (1994), Iron at high pressure: linearized-augmented-plane-wave computations in the generalized-gradient approximation, *Phys. Rev. B*, *50*(9), 6442–6445, doi:10.1103/PhysRevB.50.6442.

Sundman, B. (1991), An assessment of the Fe-O system, *J. Phase Equilibria*, *12*(2), 127–140, doi:10.1007/BF02645709.

Voèadlo, L., J. Brodholt, D. Alfè, M. J. Gillan, and G. D. Price (2000), Ab initio free energy calculations on the polymorphs of iron at core conditions, *Phys. Earth Planet. Inter.*, *117*, 123–137, doi:10.1016/S0031-9201(99)00092-8.

Voèadlo, L., D. Alfè, M. J. Gillan, I. G. Wood, J. P. Brodholt, and G. D. Price (2003), Possible thermal and chemical stabilization of body-centred-cubic iron in the Earth's core, *Nature*, *424*, 536–539, doi:10.1038/nature01829.

Williams, Q., R. Jeanloz, J. Bass, B. Svendsen, and T. J. Ahrens (1987), The melting curve of iron to 250 gigapascals: a constraint on the temperature at Earth's center, *Science*, *236*, 181–182, doi:10.1126/science.236.4798.181.

Wood, B. J. (1993), Carbon in the core, *Earth Planet. Sci. Lett.*, *117*, 593–607, doi:10.1016/0012-821X(93)90105-I.

Yoo, C. S., N. C. Holmes, M. Ross, D. J. Webb, and C. Pike (1993), Shock temperature and melting of iron at Earth core conditions, *Phys. Rev. Lett.*, *70*(25), 3931–3934, doi:10.1103/PhysRevLett.70.3931.

Yoo, C. S., J. Akella, A. J. Campbell, H. K. Mao, and R. J. Hemley (1995), Phase diagram of iron by in situ x-ray diffraction: implications for Earth's core, *Science*, *270*, 1473–1475, doi:10.1126/science.270.5241.1473.

Zarestky, J., and C. Stassis (1987), Lattice dynamics of γ-Fe, *Phys. Rev. B*, *35*(9), 4500–4502, doi:10.1103/PhysRevB.35.4500.

Y. Fei, Geophysical Laboratory, Carnegie Institution of Washington, 5251 Broad Branch Rd. NW, Washington, DC 20015, USA.

T. Komabayashi, Department of Earth and Planetary Sciences, Tokyo Institute of Technology, 2-12-1 Ookayama, Meguro, Tokyo 152-8551, Japan. (komabayashi.t.aa@m.titech.ac.jp)